Arch. Metall. Mater. **67** (2022), 4, 1469-1473

DOI: https://doi.org/10.24425/amm.2022.141076

EUNJEONG KIM[1†], SANGYOEB LEE[2†], YEONJIN JE[3], DONG PARK LEE[3], SANG JUN PARK[3], SANGHYUN JEONG[2], JOON SIK PARK[2], BYUNGMIN AHN[4*], JUN HONG PARK[1,3*]

STRUCTURAL DEFORMATION OF TUNGSTEN DISELENIDE NANOSTRUCTURES INDUCED BY OZONE OXIDATION AND INVESTIGATION OF ELECTRONIC PROPERTIES CHANGE

Tungsten diselenide (WSe_2) is one of the promising transition metal dichalcogenides (TMDs) for nanoelectronics and optoelectronics. To enhance and tune the electronic performance of TMDs, chemical functionalization via covalent and van der Waals approaches has been suggested. In the present report, the electric and structural transition of WSe_2 oxidized by exposure to O_3 is investigated using scanning tunneling microscopy. It is demonstrated that the exposure of WSe_2/high-ordered pyrolytic graphite sample to O_3 induces the formation of molecular adsorbates on the surface, which enables to increase in the density of states near the valence band edge, resulting from electric structural modification of domain boundaries via exposure of atomic O. According to the work function extracted by Kelvin probe force microscopy, monolayer WSe_2 with the O_3 exposure results in a gradual increase in work function as the exposure to O_3. Therefore, the present report demonstrates the potential pathway for the chemical functionalization of TMDs to enhance the electric performance of TMDs devices.

Keywords: Tungsten diselenide; Domain Boundary; Ozone Oxidation; Structural Deformation; Scanning Tunneling Microscopy

1. Introduction

Transition metal dichalcogenides (TMDs) have attracted great attention as potential electronic and optoelectronic platforms because of their thickness-dependent electrical and optical properties for diverse applications, such as high mobility nanoelectronics and 2D phototransistors [1-3]. Remarkably, the band structure of TMDs can be altered from indirect to direct bandgap as the number of layers decreases from multilayer to monolayer [4,5]. Furthermore, combing with molecular or atomic substitutional defects engineering, the electronic structure of TMDs can be modulated with phase deformation-induced bandgap engineering and direct/indirect doping schemes, resulting in a tunable electronic performance of nanoelectronics [6,7].

Tungsten diselenide (WSe_2) is one of the most widely studied layered semiconductors due to its tunable electronic structure and intrinsic ambipolar behavior [8,9]. Since WSe_2 has high electron mobility and high stability for electric stress, a recent study of WSe_2 has focused on thin body channel materials; thereby, atomic thickness allows efficient electrostatics and a high degree of vertical scaling [10,11]. Additionally, oxidation of WSe_2 via exposure UV-O_3 as an example of chemical functionalization has been demonstrated for hole-contact engineering at the interface of WSe_2 and metal [12-14]. In this work, we demonstrate the investigations of the structural and electronic properties of WSe_2 grown using molecular beam epitaxy (MBE) upon exposure to atomic oxygen. Using a scanning tunneling microscope (STM) and scanning tunneling spectroscopy (STS), WSe_2 oxidized by exposure to O_3 is atomically probed to elucidate the chemical transition of WSe_2 with the oxidization process. Therefore, the present report reveals that oxygen chemisorption induces the electronic/structural transition of domain boundaries as the initial reaction stage, and WSe_2 finally chemically transitioned into $WSe_{2-X}O_X$ complexes. Moreover, the shift of the Fermi level position of WSe_2 is probed using Kelvin probe force microscopy (KPFM) to extract a work function on single and bilayer WSe_2. Consequently, the present report elucidates the behavior of surface adsorption-induced chemical transition of WSe_2 at the atomic level.

[1] GYEONGSANG NATIONAL UNIVERSITY, DEPARTMENT OF MATERIALS ENGINEERING AND CONVERGENCE TECHNOLOGY, JINJU, KOREA
[2] HANBAT NATIONAL UNIVERSITY, DEPARTMENT OF MATERIALS SCIENCE AND ENGINEERING AND DEPARTMENT OF MATERIALS AND MANUFACTURING ENGINEERING, DAEJEON, KOREA
[3] GYEONGSANG NATIONAL UNIVERSITY, SCHOOL OF MATERIALS SCIENCE AND ENGINEERING, JINJU, KOREA
[4] AJOU UNIVERSITY, DEPARTMENT OF MATERIALS SCIENCE AND ENGINEERING AND DEPARTMENT OF ENERGY SYSTEMS RESEARCH, SUWON, KOREA

* Corresponding authors: yakte@gnu.ac.kr, byungmin@ajou.ac.kr
† These authors have contributed equally to this work

2. Experimental procedures

WSe_2 samples were grown on high-ordered pyrolytic graphite (HOPG) stabilized by the heating process. The growth was conducted based on prior MBE growth studies of WSe_2. During a low W flux of deposition process, the Se flux is constantly exposed at an equivalent beam pressure of 1.1×10^{-7} Torr. The deposited sample was annealed with a Se flux at 773 K for 3 mins and then re-annealed at 873 K for 7 mins. The annealed sample was cooled to 263 K under a Se flux to deposit another Se layer (~60 nm) to protect against ambient air during the transportation from the furnace to the measurement system under ultra-high vacuum (UHV).

Using electrochemically etched tungsten tips, STM and STS were performed in the Omicron VT UHV chamber. After decapping the Se adlayers from the WSe_2/HOPG samples, the mounted samples on the STM stage were cooled to 100 K by liquid nitrogen. The differential tunneling conductance (dI/dV) of WSe_2 was probed by STS using standard lock-in modulation techniques (lock-in modulation voltage: $\Delta V_{rms} = 20$ mV, $f = 500$ Hz)

3. Results and discussion

After decapping Se adlayer from the WSe_2 surface, nucleation and growth of WSe_2 across the HOPG surface with about 0.5 coverage. A large-scale image of WSe_2 on the HOPG substrate is observed using STM, as shown in Fig. 1(a). The WSe_2 is initially nucleated at the surface of HOPG; the islands of WSe_2 are formed by propagating from initial nucleation sites to form "sawtooth-shaped islands." As denoted in Fig. 1(b), the hexagonal moiré pattern at the surface of the WSe_2 monolayer is observed in a high-resolution STM image [15]. As the WSe_2 monolayer stacks on the HOPG surface, the orbitals of WSe_2 are overlapped with the orbital of the topmost HOPG layer. Therefore, a hexagonal array of protrusions results from the periodic potential wells of orbital overlapping. The atomic-resolved STM image of WSe_2 captured at a sample bias (V_{sample}) of V (80 *p*A) is obtained with periodic bright spots corresponding to the layer of Se atoms. The spacing between Se atoms measured is statistically about 0.33 nm, similar to the previously reported lattice parameters of WSe_2 [16,17].

After confirmation of bare WSe_2 surface, using STM, the WSe_2 samples are exposed to O_3 produced by UV-O_3 generator for 1 min in a separated dosing chamber. In contrast, the pressure of the dosing chamber maintains about 2×10^{-4} torr at 300 K. The exposure of the WSe_2/HOPG sample to O_3 induces the existence of molecular adsorbates on the surface, as shown in the large-scale STM image in Fig. 1(c). It can be hypothesized that the adsorbates are mostly oxygen-containing complex or hydrocarbon. To elucidate the electronic effect of O_3-induced

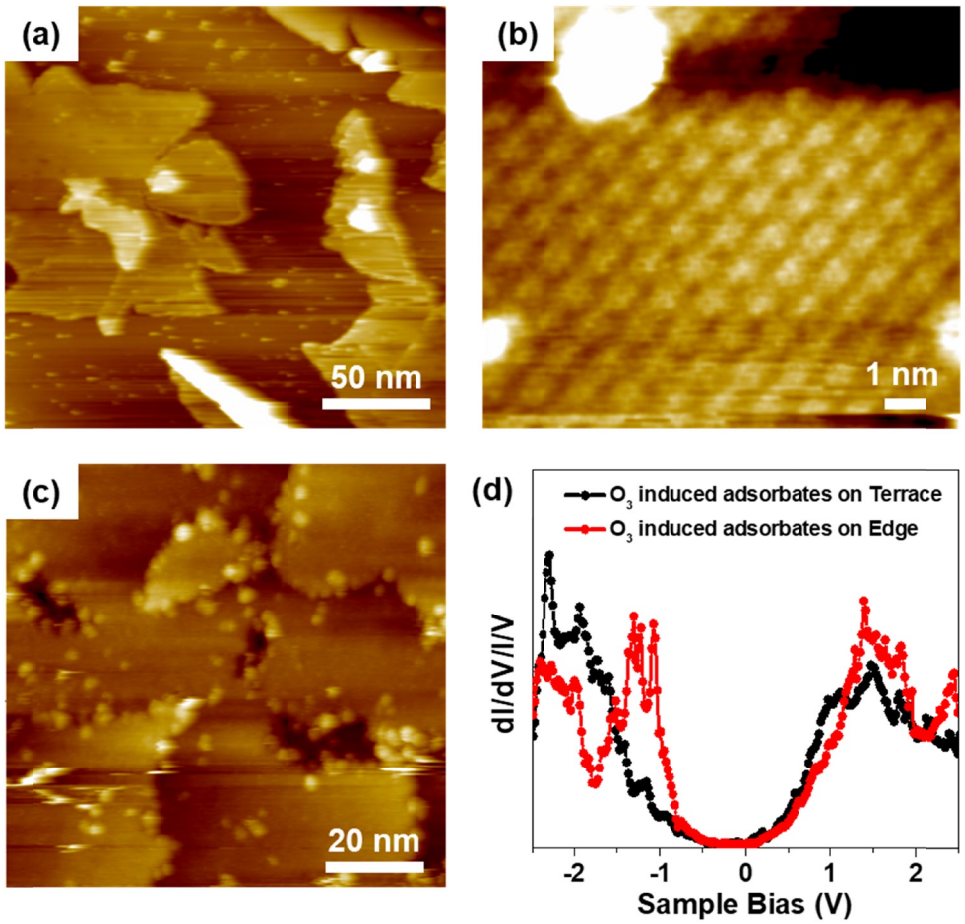

Fig. 1. (a) Large-area STM image of ML WSe_2 grown on the HOPG substrate ($V = 2$ V, $I_T = 20$ pA); (b) high-resolution STM image of WSe_2 ML ($V = 1.0$ V, $I_T = 80$ pA); (c) STM image of WSe_2 after the O_3 exposure ($V = 2$ V, $I_T = 20$ pA); (d) STS spectra of O_3 induced adsorbates

adsorption on WSe_2, STS is performed. In Fig. 1(d), the black spectra are assigned to the electronic structure of adsorbates on the WSe_2 terrace, while the red spectra correspond to the electronic structure of adsorbates at the WSe_2 edge. Although the narrow band structure is observed in both sites with a large band edge density of states (DOS), the O_3 induced adsorbates at the WSe_2 edges have larger DOS near valence band edge than adsorbates on the WSe_2 terrace. The previous reports reveal that large DOS is associated with transition metal termination due to the incomplete structural configuration of atomic structure at the TMDC edge [18]. Therefore, as this defect associated DOS is mixed with DOS of adsorbates in tunneling signal, resulting in large DOS at the band edge in STS.

Exposure of WSe_2 to O_3 induces the electronic transition of domain structure in WSe_2, consistent with observable bias dependence of STM image. In Fig. 2(a), triangle-shaped domain boundaries are clearly shown with blight protrusion at a sample bias of –1.5 V, consistent with the filled state image. Conversely, these domain boundaries are not observable in the empty state image of Fig. 2(b) obtained at 1.5 V. To bias dependence of domain boundaries at the atomic scale; the sample imaging bias decreases to 1.0 V to approach the STM tip to the surface. The filled state image obtained at –1.0 V reveals Se atoms array in electrically brightened domain boundaries, as shown in the white arrow in Fig. 2(c). It is noted that although the empty state image of Fig. 2(d) also shows the triangular domain boundaries, it is less distinct than filled states. It can be hypothesized that the atomic O modified domain boundaries have donated electrons during tunneling between STM tips and samples. The local density of state (LDOS) of atomic O exposed ML WSe_2 is measured using STS. The red circle is marked on the triangular domain boundaries, indicating the O_3-modified domain structures, while the black circle is marked internal domains. From the dI/dV spectra in Fig. 2(e), the red spectra obtained on triangle boundaries has larger LODS at both valence band (VB) and conduction band (CB) edges, as shown in green arrows, compared to the black spectra measured at off the triangle boundaries. Thus, the atomic-scaled STS curves are consistent with the bias dependence of atomic O modified domain boundaries shown in Figs. 2(a-d).

To elucidate thermal stability of the O_3 induced domain structure transition in WSe_2, the WSe_2 samples are additionally exposed to O_3 for 5 min under the same conditions, then are annealed at 673 K for 30 min under the ultra-high-vacuum (P: 2×10^{-10} torr). Bias-dependent STM characterizations of triangular domain boundary in WSe_2 can be observed in the STM image of Fig. 3(a). As shown in zoomed-in image of Fig. 3(b), triangle-shaped features along the domain are detected in the WSe_2 samples, consistent with the high-thermal stability of O_3-induced domain transition. To elucidate the impact of O_3 induced transition on the electronic structure of WSe_2, the band structure of the WSe_2 monolayer (ML) is probed using STS, as shown in Fig. 3(c). The bare WSe_2 ML has about 2.09 eV electronic bandgap, consistent with the previous reports [19]. After exposure of WSe_2 to O_3 for 1min at 300 K, the bandgap of WSe_2 ML decreases significantly to about 1.16 eV. With further exposure to O_3 for 5 min, an additional reduction of WSe_2 ML bandgap is observed about 0.88 eV. As shown in Fig. 2(e), O_3 exposure induces the structural/electronic transition of the domain structure with an increase in DOS at VB and CB. As shown in previous reports [20], atomic oxygen atoms are produced by dissociation of O_3 into O_2 and O. Therefore, it can be hypothesized that as the atomic structure of WSe_2 is exposed to atomic oxygen, initially, domain boundaries of WSe_2 react with O. Afterwards, oxidization of WSe_2 is propagate from domain boundaries to internal domains, consistent with the formation of $WSe_{2-x}O_x$ complexes. Since the formed $WSe_{2-x}O_x$ complexes have a large density of defects, the structural incomplete induces

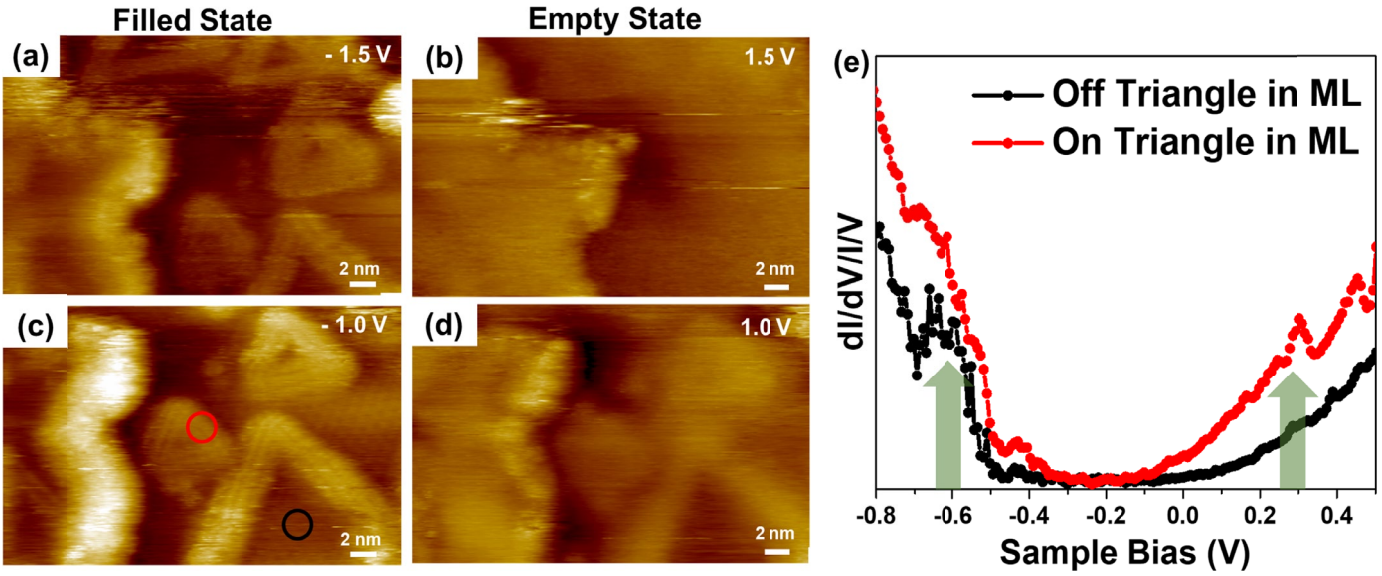

Fig. 2. (a) STM image of ML WSe_2 in filled state at a sample bias of –1.5 V (I_T = 100 pA); (b) Empty state image obtained at 1.5 V (I_T = 100 pA); (c) Filled state image obtained at –1.0 V (I_T = 100 pA); (d) Empty state image obtained at 1.0 V (I_T = 100 pA); (e) STS spectra on the O_3 modified domains boundary marked by a red-circle and the rest of the area marked by black-circle

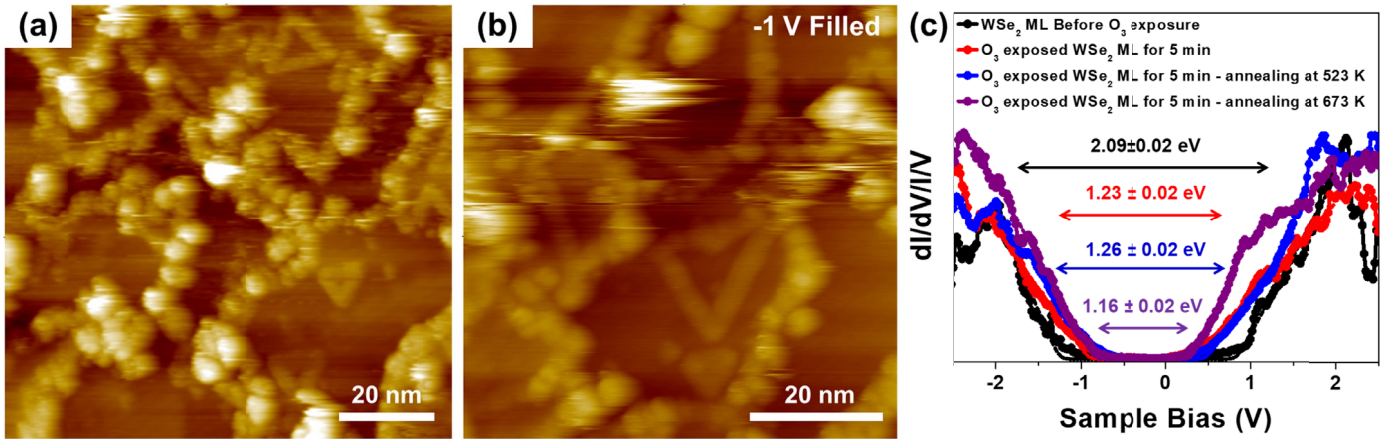

Fig. 3. (a) STM image of WSe_2 exposed to O_3 for 6 min ($V = -1.5$ V, $I_T = 20$ pA; (b) Zoomed-in STM image for the triangular domain ($V = -1$ V, $I_T = 80$ pA); (c) STS spectra of WSe_2 as exposure to O_3

large defect states in the band structure, consistent with a narrow bandgap.

KPFM is employed to extract a work function on single- and bilayer WSe_2. The WSe_2 is transferred by mechanical exfoliation of bulk WSe_2 onto thermally grown SiO_2 substrates. A topographical image of the entire WSe_2 flake is shown in Fig. 4(a). After confirmation of the position of the WSe_2 flake, KPFM images are obtained, as shown in Fig. 4(b). Contact potential difference images are displayed in Figs. 4(c) and 4(d), which corresponded to O_3 exposed for 2 min and O_3 exposed for 6 min, respectively. In order to tract the Fermi level position upon exposure to atomic oxygen, contact potential difference is measured by KPFM. Afterward, work functions of samples (Φsample) are extracted, as shown in the following equation [21],

$$V_{CPD} = \frac{\Phi sample - \Phi tip}{e}$$

where e is the elementary charge. The overall transition of work functions for each procedure are summarized in Fig. 4(e). After exposure of WSe_2 to O_3 for 2 min, the work function increases about 0.3 eV, consistent with STM/STS results shown above. Moreover, the O_3 exposure for 6 min induces the additional in-

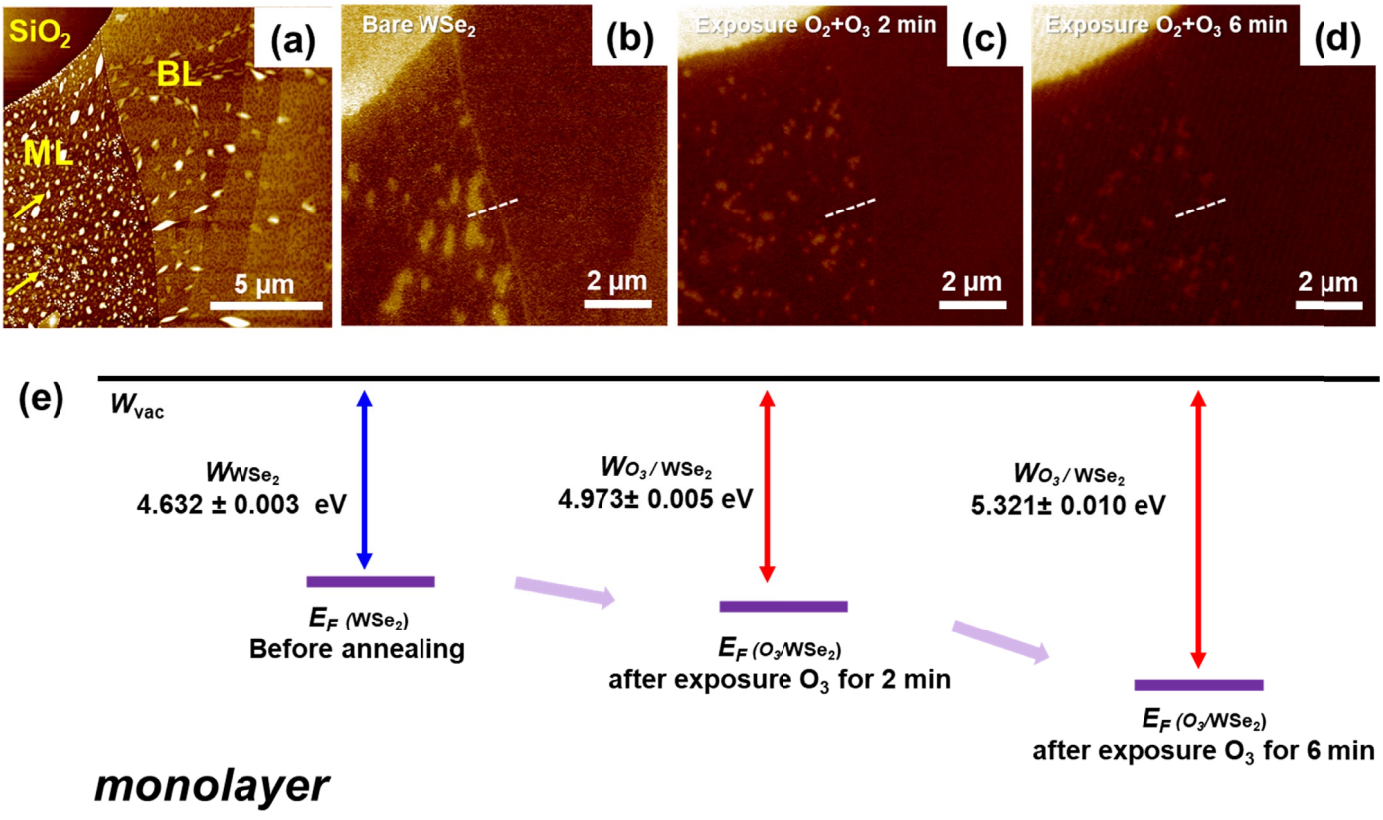

Fig. 4. (a) AFM topography image of entire WSe_2 flake consisting of single- and bilayer. KPFM images of (b) bare WSe_2; (c) WSe_2 exposed to $O_2 + O_3$ for 2 min; (d) WSe_2 exposed to $O_2 + O_3$ for 6 min; (e) Summary of extracted work function of WSe2 ML, as exposure to O_3

crease of a work function to 5.321 ± 0.01 eV. This suggests the Fermi level of WSe_2 shifts to the valence band with exposure O_3, consistent with p-type behavior. It can be hypothesized that the exposure to O_3 results in a chemical transition to the formation of WO_x with lattice distortion, consistent with previous reports [22].

4. Conclusions

The electric and structural transition of WSe_2 oxidized by exposure to UV-ozone is investigated using surface probing. After confirmation of bare MBE grown WSe_2 surfaces, STM reveals that the WSe_2/HOPG sample exposure to O_3 induces the existence of molecular adsorbates on the surface. It is noted that the O_3 induced adsorbates at the WSe_2 edges have larger DOS near valence band edge than adsorbates on the WSe_2 terrace due to the defect of the WSe_2 domain structure. As exposure of WSe_2 surface to atomic O, adsorption of atomic O induces the chemical/electric modification of domain boundaries, consistent with STM bias dependence. The electric transition of O_3 modified domain boundaries can be confirmed by STS, consistent with an increase of LDOS at both VB and CB. In addition, a work function on single- and bi-layer WSe_2 is extracted using KPFM. The extracted work function (Φ_S) of monolayer WSe_2 is increased with the O_3 exposure, resulting in the Fermi level shift to the valence band. Therefore, the present results suggest the elucidation of chemical and electric functionalization of TMDs, using molecular and atomic adsorption on the surfaces.

Acknowledgments

This work was supported by the National Research Foundation of Korea (NRF) grant funded by the Korea government (MSIT) (No. 2021R1C1C1012209 and 2020R1A4A4079397).

REFERENCES

[1] R.S. Chen, C.C. Tang, W.C. Shen, Y.S. Huang, Nanotechnology **25**, 451706 (2014).

[2] Q.H. Wang, K. Kalantar-Zadeh, A. Kis, J.N. Coleman, M.S. Strano, Nat. Nanotechnology **7**, 699 (2012).

[3] W. Zhang, M.H. Chiu, C.H. Chen, W. Chen, L.J. Li, A. T.S. Wee, ACS Nano **8**, 8653 (2014).

[4] S.L. Howell, D. Jariwala, C.C. Wu, K.S. Chen, V.K. Sangwan, J. Kang, T.J. Marks, M.C. Hersam, L.J. Lauhon, Nano Lett. **15**, 2278 (2015).

[5] W. Zhou, J. Chen, Z. Yang, J. Liu, F. Ouyang, Phys. Rev. B **99**, 075160 (2019).

[6] Q. Zhang, A.T.S. Wee, Q. Liang, X. Zhao, M. Liu, ACS Nano **15**, 2165 (2021).

[7] E. Blundo, M. Felici, T. Yildirim, G. Pettinari, D. Tedeschi, A. Miriametro, B. Liu, W. Ma, Y. Lu, A. Polimeni, Phys. Rev. Res. **2**, 012024 (2020).

[8] X. Duan, C. Wang, Z. Fan, G. Hao, L. Kou, U. Halim, H. Li, X. Wu, Y. Wang, J. Jiang, A. Pan, Y. Huang, R. Yu, X. Duan, Nano Lett. **16** 264 (2016).

[9] Z. Wang, Q. Li, Y. Chen, B. Cui, Y. Li, F. Besenbacher, M. Dong, NPG Asia Mater. **10**, 703 (2018).

[10] L. Kong, X. Zhang, Q. Tao, M. Zhang, W. Dang, Z. Li, L. Feng, L. Liao, X. Duan, Y. Liu, Nat. Commun. **11**, 1 (2020).

[11] P. Debashis, T.Y.T. Hung, Z. Chen, NPJ 2D Mater. Appl. **4**, 1 (2020).

[12] S. Yang, G. Lee, J. Kim, ACS Appl. Mater. Interfaces **13**, 955 (2021).

[13] M. Yamamoto, S. Dutta, S. Aikawa, S. Nakaharai, K. Wakabayashi, M.S. Fuhrer, K. Ueno, K. Tsukagoshi, Nano Lett. **1**5, 2067 (2015).

[14] Y.C. Lin, B.M. Bersch, R. Addou, K. Xu, Q. Wang, C.M. Smyth, B. Jariwala, R.C. Walker, S.K. Fullerton-Shirey, M.J. Kim, R.M. Wallace, J.A. Robinson, Adv. Mater. Interfaces **7**, 2000422 (2020).

[15] R. Yue, Y. Nie, L.A. Walsh, R. Addou, C. Liang, N. Lu, A.T. Barton, H. Zhu, Z. Che, D. Barrera, L. Cheng, P.R. Cha, Y.J. Chabal, J.W.P. Hsu, J. Kim, M.J. Kim, L. Colombo, R.M. Wallace, K. Cho, C.L. Hinkle, 2D Mater. **4**, 045019 (2017).

[16] P. Mallet, F. Chiapello, H. Okuno, H. Boukari, M. Jamet, J.Y. Veuillen, Phys. Rev. Lett. **125**, 036802 (2020).

[17] R. Addou, C.M. Smyth, J.Y. Noh, Y.C. Lin, Y. Pan, S.M. Eichfeld, S. Fölsch, J.A. Robinson, K. Cho, R.M. Feenstra, R.M. Wallace, 2D Mater. **5**, 025017 (2018).

[18] A. Banerjee, H. Bhunia, A.J. Pal, J. Phys. D Appl. Phys. **54**, 105106 (2021).

[19] H.J. Liu, L. Jiao, L. Xie, F. Yang, J.L. Chen, W.K. Ho, C.L. Gao, J.F. Jia, X.D. Cui, M.H. Xie, 2D Mater. **2**, 034004 (2015).

[20] R.A. Ruehrwein, J.S. Hashman, J. Chem. Phys. **30**, 823 (1959).

[21] Y. Rosenwaks, R. Shikler, T. Glatzel, S. Sadewasser, Phys. Rev. B Condens. Matter. **70**, 085320 (2004).